Supporting Information

# Design and Synthesis of Room Temperature Stable Li-Argyrodite Superionic Conductors *via* Cation Doping

Zhuoran Zhang[a,b,†], Yulong Sun[a,†], Xianbao Duan[c], Linfeng Peng[a], Huanhuan Jia[a,b], Yunyang Zhang[a,b], Bin Shan[b], and Jia Xie[a,*]

[a] *State Key Laboratory of Advanced Electromagnetic Engineering and Technology, School of Electrical and Electronic Engineering, Wuhan 430074, China.*

[b] *State Key Laboratory of Materials Processing and Die & Mould Technology, School of Materials Science and Engineering, Huazhong University of Science and Technology, Wuhan 430074, China*

[c] *School of Materials Science and Engineering, Wuhan Institute of Technology, Wuhan 430073, Hubei, China*

† These authors contributed equally to this work.

**Table S1.** Energy difference ($\Delta E$) of various ionic substitutions (Al, B, Ge, Si) argyrodites and pure $Li_7PS_6$ between HT and LT phase

| *substitution* | $E_{HT}$ (*eV/Å*) | $E_{LT}$ (*eV/Å*) | $\Delta E(E_{HT}–E_{LT})$ (*eV/Å*) | *Stable phase* |
|---|---|---|---|---|
| None | –234.79627 | –234.82979 | –0.03352 | LT phase |
| Si | –234.95776 | –234.78552 | 0.17224 | HT phase |
| Ge | –230.67633 | –230.52328 | 0.15305 | HT phase |
| Al | –230.05914 | –231.27840 | –1.21926 | LT phase |
| B | –235.19432 | –235.28478 | –0.09046 | LT phase |

**Table S2**. Composition dependence of the Ionic Conductivity of Cold-Pressed Powder at Room Temperature

| $Li_{7.2}B_{0.1}P_{0.9}S_6$ | $Li_{7.2}Al_{0.1}P_{0.9}S_6$ |
|---|---|
| Ionic conductivityσ/ S $cm^{-1}$ | Ionic conductivityσ/ S $cm^{-1}$ |
| $9.88\times10^{-6}$ | $8.52\times10^{-5}$ |

**Table S3**. Rietveld refinements of X-ray diffraction data for $Li_{7.25}Ge_{0.25}P_{0.75}S_6$ at 298 K.

| $Li_{7.25}Ge_{0.25}P_{0.75}S_6$ structure from X-ray diffraction data (space group $F\bar{4}3m$) ;<br>$a$ = 9.9543(1) Å<br>Fit residuals ($R_{wp}$, $R_{exp}$, $\chi^2$ ): 6.46%, 4.72%, 2.86 | | | | | | |
|---|---|---|---|---|---|---|
| Atom | Site | *x* | *y* | *z* | Occ. | $U_{iso}$/ Å$^2$ |
| Li1 | 48h | 0.823(2) | 0.498(1) | 0.676(2) | 0.60(1) | 0.1043(9) |
| S1 | 16e | 0.623(1) | *x*(S1) | *x*(S1) | 1 | 0.0244(4) |
| S2 | 4c | 0.250 | *x*(S2) | *x*(S2) | 1 | 0.0164(9) |
| S3 | 4a | 0 | *x*(S3) | *x*(S3) | 1 | 0.0302(1) |
| Ge1 | 4b | 0.500 | *x*(Ge1) | *x*(Ge1) | 0.23(2) | 0.0531(3) |
| P1 | 4b | *x*(Ge1) | *x*(Ge1) | *x*(Ge1) | 1-Occ.(Ge1) | $U_{iso}$（Ge1） |

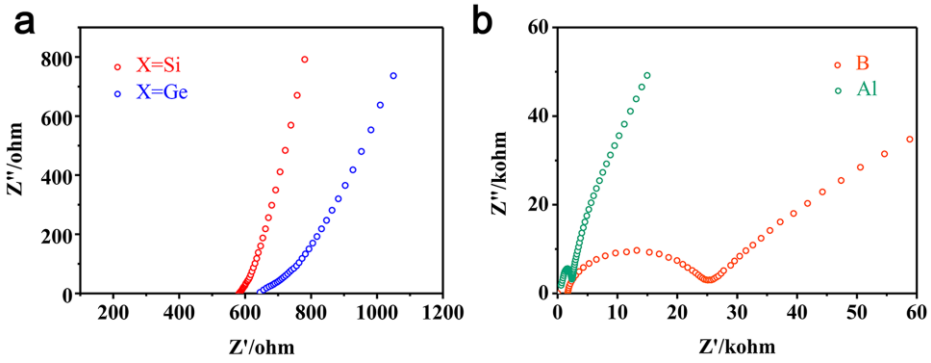


**Figure S1. a.** Nyquist plots of $Li_{7.1}M_{0.1}P_{0.9}S_6$ (*M* = Si, Ge), **b**. Nyquist plots of $Li_{7.2}N_{0.1}P_{0.9}S_6$ (*N* = B, Al) at room temperature.

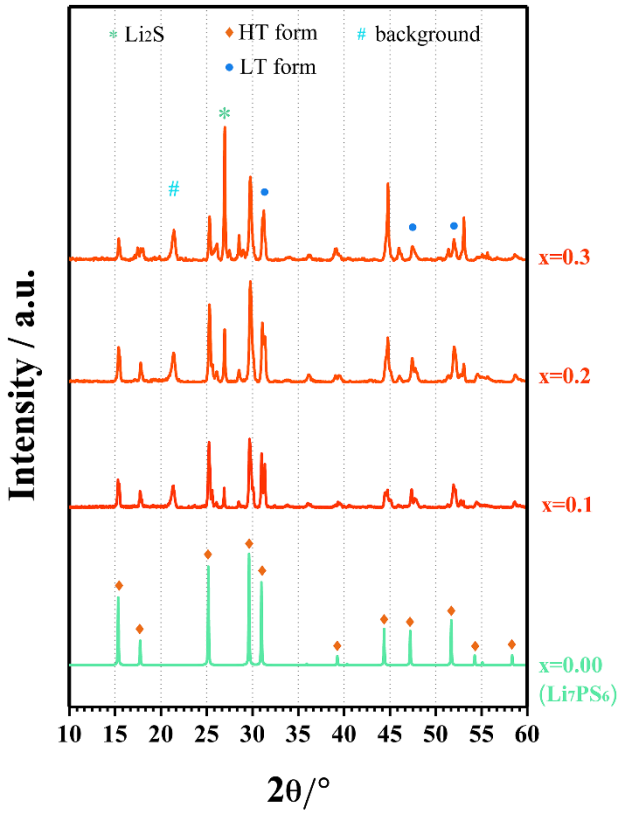


**Figure S2**. X-ray diffraction (XRD) patterns of $Li_{7+2x}Al_xP_{1-x}S_6$ (x = 0.1, 0.2, 0.3).

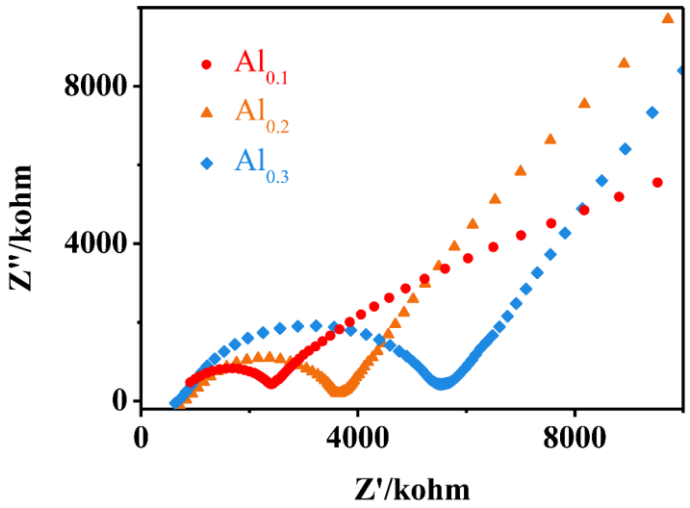


**Figure S3**. Nyquist plots of $Li_{7+2x}Al_xP_{1-x}S_6$ (x = 0.1, 0.2, 0.3).

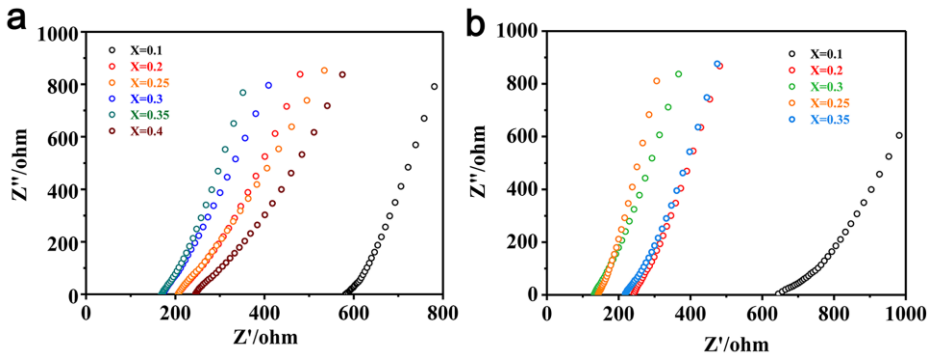


**Figure S4.** Nyquist plots of $Li_{7+x}M_xP_{1-x}S_6$ (*M* = Si, Ge , *x* = 0.1–0.4) at room temperature. **a.** *M* = Si. **b.** *M* = Ge.

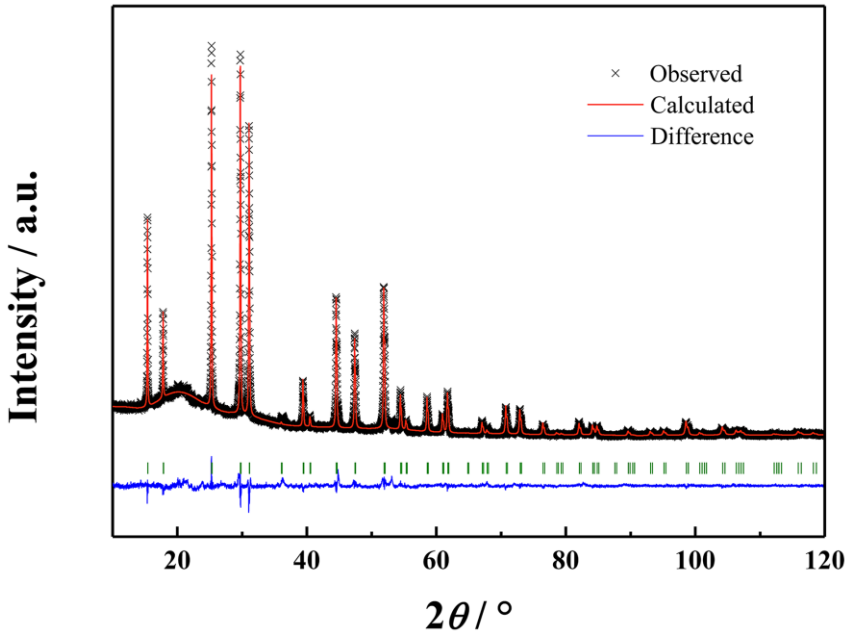


**Figure S5**. Rietveld refinement pattern of $Li_{7.25}Ge_{0.25}P_{0.75}S_6$ at 298 K. Experimental data are shown as points; Red: calculated intensities; black: observed intensities; blue: difference profile. The green markets indicate the positions of the diffraction lines.

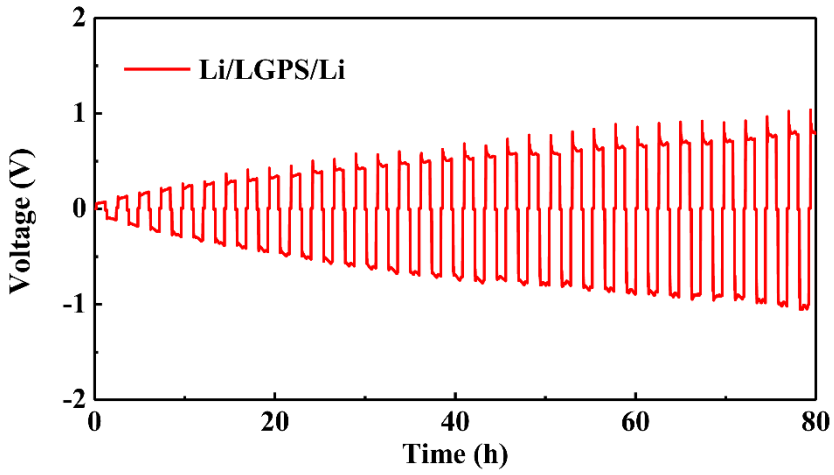


**Figure S6**. Potential profiles during galvanostatic cycling for a Li/LGPS/Li cell.

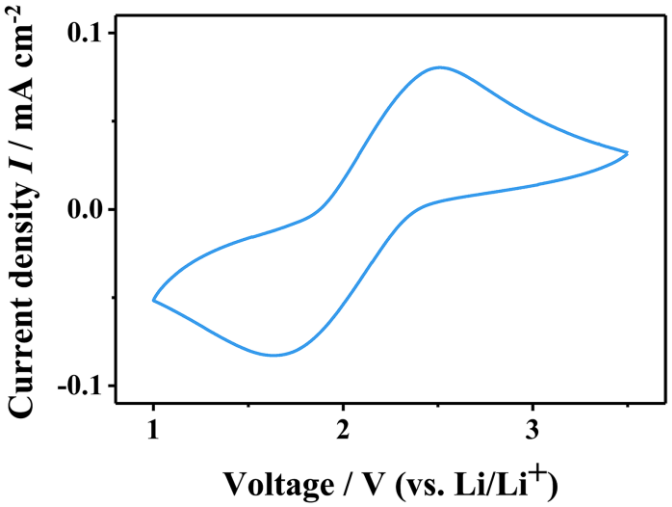


**Figure S7.** Cyclic voltammogram for a Li/$Li_{7.25}Si_{0.25}P_{0.75}S_6$/$TiS_2$ cell; from 1 to 3.5 V at a scan rate of 1 mV $s^{-1}$.

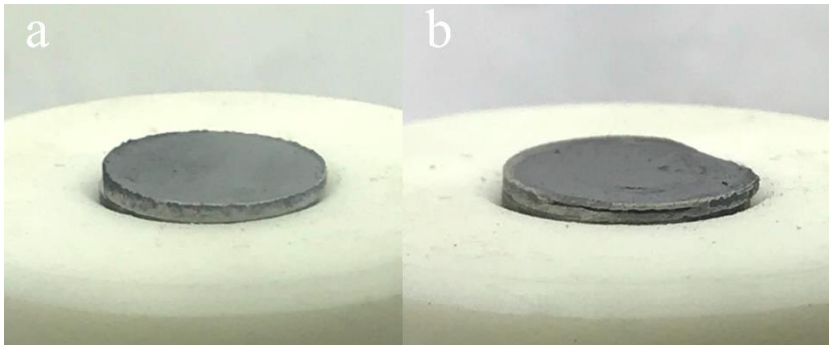


**Figure S8.** Photographs of $TiS_2$/SE/Li all-solid-state cell before (a) and after (b) charge-discharge cycle.